A Thoria and Thorium Uranium Dioxide Nuclear Fuel Performance Model Prototype and Knowledge Gap Assessment

J. S. Bell[2]
Department of Chemistry
and Chemical Engineering,
Royal Military College of Canada,
P.O. Box 17000,
Station Forces,
Kingston, ON K7K 7B4, Canada
e-mail: john.s.bell@cnl.ca

P. K. Chan[1]
Department of Chemistry
and Chemical Engineering,
Royal Military College of Canada,
P.O. Box 17000,
Station Forces,
Kingston, ON K7K 7B4, Canada
e-mail: Paul.Chan@rmc.ca

A. Prudil[3]
Department of Chemistry
and Chemical Engineering,
Royal Military College of Canada,
Station Forces,
P.O. Box 17000
Kingston, ON K7K 7B4, Canada
e-mail: Andrew.Prudil@cnl.ca

Thorium-based fuel cycles can improve fuel sustainability within the nuclear power industry. The Canadian supercritical water-cooled reactor (SCWR) concept uses this path to achieve the sustainability requirement of the Gen-IV Forum. The study of thorium dioxide/thoria ThO_2-based fuel irradiation behavior is significantly less advanced than that of uranium dioxide (UO_2) fuel, although ThO_2 possesses superior thermal conductivity, thermal expansion, higher melting temperature, and oxidation resistance that may improve both fuel performance and safety. The fuel and sheath modeling tool (FAST), a fuel performance model for UO_2 fuel, was developed at the Royal Military College of Canada (RMCC). FAST capability has been extended to include thoria (ThO_2), thorium uranium dioxide ($Th,U)O_2$, and thorium plutonium dioxide ($Th,Pu)O_2$ as fuel pellet materials, to aid in designing and performance assessment of Th-based fuels, including SCWR ($Th,Pu)O_2$ fuel. The development and integration of ThO_2 and ($Th,U)O_2$ models into the existing FAST model led to the multipellet material FAST (MPM-FAST). Model development was performed in collaboration between RMCC and Canadian Nuclear Laboratories (CNL). This paper presents an outline of the ThO_2 and ($Th,U)O_2$ MPM-FAST model, a comparison between modeling results with postirradiation examination (PIE) data from a test conducted at CNL, and an account of the knowledge gap between our ability to model ThO_2 and ($Th,U)O_2$ fuel compared to UO_2. Results are encouraging when compared to PIE data. [DOI: 10.1115/1.4039778]

Keywords: nuclear fuel and materials, next generation reactors and advanced reactors, SCWR, thoria, thorium uranium dioxide, fuel performance

1 Introduction

The use of thorium-based fuels is advancing along several fronts. This work is motivated by Canada's participation in the Gen-IV Forum and is being led by CNL in the development of a pressure tube, heavy water moderated supercritical water-cooled reactor (SCWR) concept described by McDonald et al. [1] and Yetisir et al. [2]. One of the proposed conceptual designs is the use of a thorium-based fuel cycle, as this would address the GEN-IV Forum requirement of greater sustainability in nuclear power generation by providing fuel options not dependent on uranium. Specifically, the proposed fuel is thorium–plutonium dioxide ($(Th,Pu)O_2$) with 13 wt % Pu. Beyond SCWR fuel, this work is motivated by ongoing efforts to expand pressurized heavy water reactor (PHWR) fueling options to include Th-based fuel cycles [3]. This is demonstrated by the recent agreement in principle in the development of the advanced fuel CANDU Reactor between SNC-Lavalin, China National Nuclear Corporation, and Shanghai Electric [4]. Additional interest in establishing Th-based commercial fuel is shown in India's "3-stage" nuclear power strategy [5] and Thor Energy [6] conducting research to support the use of Th-based fuel for light-water reactor designs.

As the SCWR concept design matures, and Th-based fuel moves toward commercialization, more detailed analysis of how this fuel type behaves during irradiation will be required. Tools for this type of analysis for uranium dioxide (UO_2) fueled PHWR elements include ELESTRES for normal operating conditions (NOC) and ELOCA for transient conditions and are described by Chassie et al. [7] and Williams [8], respectively. These fuel performance codes have many similarities with their internationally developed counterparts including FRAPCON/FRAPTRAN ([9,10]), FALCON [11], TRANSURANUS [12], ALCYONE [13], and MOOSE/BISON [14]. These fuel performance codes calculate important parameters to assess fitness for service including fuel temperature, sheath strain, pellet deformation, fission gas (FG) production, fission gas release (FGR) to the element free volume, and internal gas pressure.

Specifically, this paper will report on the development of the thoria (ThO_2) and thorium uranium dioxide ($(Th,U)O_2$) fuel performance model [15]. The development of this model was accomplished in collaboration with Canadian Nuclear Laboratories (CNL) (formerly Atomic Energy of Canada Limited), under their Thoria Roadmap project, summarized by Floyd et al. [16]. This project examined the state of commercial readiness of Th-based nuclear fuel technology and addresses identified science and technology gaps. The expectation was that the $(Th,U)O_2$ model will be limited compared to UO_2-based models due to the smaller database of $(Th,U)O_2$ irradiation experiments. By building the model at this time, these limitations provide a knowledge gap assessment of the irradiation behavior of ThO_2 and $(Th,U)O_2$. In developing the multipellet material FAST (MPM-FAST), $(Th,U)O_2$ specific references and experimental works were used when available. When there is insufficient $(Th,U)O_2$ data, MPM-FAST relies on the UO_2 models implemented in the fuel and sheath modeling tool (FAST) [17]. This work identifies material properties and models that were added and modified to account for the use of $(Th,U)O_2$. A brief summary of the knowledge gap assessment is discussed, and the modeling results are also compared with postirradiation examination (PIE) data

[1]Corresponding author.
[2]Present address: Nuclear Safety Experiments Branch, Canadian Nuclear Laboratories Chalk River, ON K0J 1J0, Canada.
[3]Present address: Computational Techniques Branch, Canadian Nuclear Laboratories Chalk River, ON K0J IJ0, Canada.
Manuscript received June 30, 2017; final manuscript received February 25, 2018; published online January 24, 2019. Assoc. Editor: Jovica R. Riznic.

from an irradiation test conducted at CNL, described by Corbett et al. [18].

2 $(Th,U)O_2$ Model Development

Work performed at the Royal Military College of Canada (RMCC) has developed UO_2 fuel performance models using the commercially available finite element solver software COMSOL MULTIPHYSICS [17,19,20]. The latest in this series of models is FAST, which has undergone proof-of-concept validation against both NOC and transient conditions for Canadian PHWR fuel [21,22]. FAST provides a numerical solution to the heat transport, deformation, and fission gas release equations, using the finite element method on a half-axially symmetric UO_2 pellet stack and sheath (Zircaloy-4) geometry. By adding the thermal-physical properties and the known irradiation behaviors of ThO_2 and $(Th,U)O_2$ to FAST, a model for Th-based fuel can be developed. In order to establish confidence in the model and leverage existing irradiation data, it is desirable to demonstrate that the model is capable of replicating existing PIE results from Th-based fuel irradiations prior to applying it to SCWR fuel (which adds additional complexity due to its high plutonium content, high specific power, high aspect ratio geometry, different cladding materials, and higher coolant temperatures). Thus, this effort is seen as an incremental step in producing a fuel performance model for SCWR fuel and other advanced reactor concepts.

With the addition of Th-based pellet material models to UO_2 FAST, the fuel performance model will be referred to as MPM-FAST. The Zircaloy-4 model (the sheath heat transport and deformation) within MPM-FAST was not modified from FAST and is described in Prudil's work [17,21,22].

Canadian PHWR fuel bundles are approximately 0.1 m in diameter and consist of concentric rings of cylindrical fuel elements (each element is $\sim$0.013 m in diameter). The elements are welded to end plates at either end of the bundle and separation between elements is maintained with spacer pads. The version of FAST used in the development of MPM-FAST assumes axial symmetry of a cylindrical fuel element to reduce the model to two dimensions [21]. Due to the limited axial change in flux and coolant temperature along the length of a 0.5 m fuel element, it is further assumed that the irradiation behavior of one pellet is representative of all pellets within a fuel element (although the capability of modeling axially varying of irradiation conditions is preserved for future use with SCWR fuel designs). The resulting simplified MPM-FAST geometry consists of a half-pellet with the corresponding section of the sheath with azimuthal symmetry and periodic boundary conditions applied, as shown in Fig. 1. A sample of the meshed geometry is included on the right side of Fig. 1.

In Fig. 1, the bottom pellet land and sheath are assumed fixed in the axial direction. With careful examination, it can be seen that the top of the sheath exceeds the height of the pellet. This height difference is representative of the free axial gap divided by the number of pellets in the stack. Once the top of the pellet approaches the height of the sheath, the model applies a contact load representative of pellets stack contacting the end-caps, the full details are discussed by Prudil [17]. The two primary phenomena that a fuel performance model calculates are fuel temperature and deformation. In Fig. 1, the pellet-to-clad gap remains unmeshed due to the very high aspect ratio and is instead treated 1-dimensionally on the pellet and cladding boundaries. The equations modeling the behavior in the meshed regions of the pellet are discussed in Secs. 2.1 and 2.2. The approximate dimensions of Canadian PHWR fuel are 4.0×10^{-4} m thick Zircaloy-4 sheath, initial pellet-to-sheath gap of 5.0×10^{-5} m, and 1.6×10^{-2} m long fuel pellets. Once inserted into a pressurized fuel channel, the sheath quickly comes into contact with the fuel due to thermal expansion and elastic compression. A one-dimensional heat-transfer model accounts for the heat-flux through the gap with a locally varying heat-transfer coefficient, which enables the gap to go unmeshed, and is solved for each time-step. The model tracks

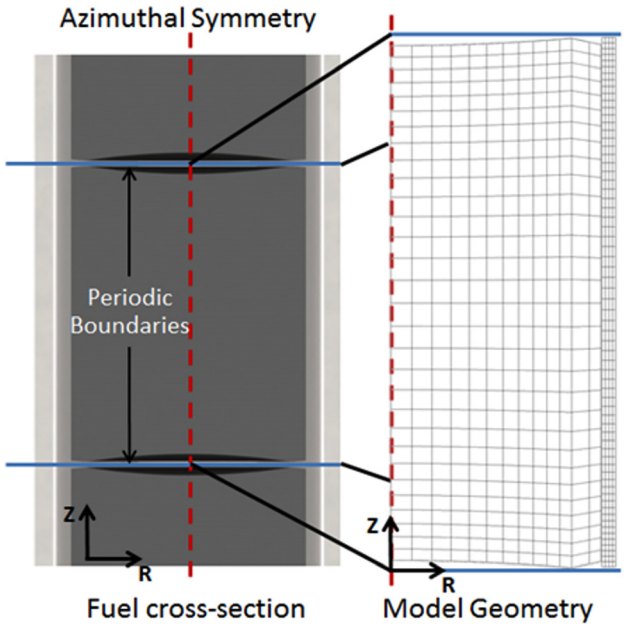

Fig. 1 Fuel-cross section with overlaid boundary conditions (left) and the MPM-FAST model geometry and mesh (right) [17]

the volume and composition of the gas, and how the deformation of the pellet and sheath alters the internal void volume available to the gas during the irradiation. Internal pressure of the fuel element is determined using a variation on the ideal gas law. With this gas pressure and the contact pressure between the sheath and the pellet (calculated using the contact penalty method), gap heat transport can be approximated as a one-dimensional steady-state heat transfer. A full description of this work can be found in Prudil's thesis [17].

2.1 Heat Transport. MPM-FAST calculates temperatures within the pellet mesh by approximating the solution to heat transport by conduction through a solid; the general differential equation is given in the following equation:

$$\rho C_p \frac{\partial T}{\partial t} = \nabla \cdot (k \nabla T) + Q \tag{1}$$

T is the temperature (K), t is the time (s), and ρ is the pellet density (kg/m^3). The initial $(Th,U)O_2$ density used in MPM-FAST is taken from fuel manufacturing data, and the changes in density found during the deformation calculation are discussed below. C_p is the specific heat capacity of $(Th,U)O_2$ (J/(K kg)); since this is an NOC model with large time steps (i.e., near thermal equilibrium), the specific heat has little effect on the modeling results and will not be discussed further.

Two correlations of $(Th,U)O_2$ unirradiated thermal conductivity (k_0 in W/(m K)) have been tested in MPM-FAST; both are presented in the form of a semi-empirical correlation given in the following equation:

$$k_0 = \frac{1}{\mathbf{A} + \mathbf{B}T} \tag{2}$$

A and **B** are dependent on the proportion of uranium mixed with thorium. The first of the $(Th,U)O_2$ models used a correlation presented by Belle and Berman for 100% theoretical density $(Th,U)O_2$ up to 0–30% UO_2 content below 2200 K, with the $\mathbf{A_a}$ and $\mathbf{B_a}$ components in the following equation [23]:

$$\mathbf{A_a} = \frac{1}{46.948 - 112.072\mathbf{M_U}}$$
$$\mathbf{B_a} = 1.597 \times 10^{-4} + 6.736 \times 10^{-4}\mathbf{M_U} - 2.155 \times 10^{-3}\mathbf{M_U^2} \tag{3}$$

$\mathbf{M_U}$ is the mole percent of UO_2 present in the ceramic mixture. The use of this thermal conductivity is similar to the work by Long et al. on a Th version of FRAPCON [24].

The second thermal conductivity correlation tested in the model was presented by Bakker et al. for thermal conductivity of $(Th_{1-y},U_y)O_2$ at 95% theoretical density, where y is the wt % of U up to 10% ($0 \leq \mathbf{y} \leq 0.1$) and temperatures between 300 and 1800 K (outlined in Eq. (4)) [25]

$$\begin{aligned}\mathbf{A_b} &= 0.0004195 + 1.112\mathbf{y} - 4.499\mathbf{y}^2 \\ \mathbf{B_b} &= 0.0002248 - 0.000917\mathbf{y} + 0.004164\mathbf{y}^2\end{aligned} \tag{4}$$

A correction factor is applied to the Bakker correlation to make it applicable to 100% dense $(Th,U)O_2$.

During irradiation, the Lucuta model (k_{Lucuta}) is applied to both of the examined correlations in order to account for changes in thermal conductivity [26]. The Lucuta model is based on the premise that the effects of irradiation, accumulation of fission products, changes in oxygen stoichiometry, and porosity on unirradiated thermal conductivity (k_0) can be accounted for by applying a series of unitless multiplication factors shown in Eq. (5). Although this model was developed for UO_2 fuel with simulated burnup (fuel with nonradioactive isotopes added in proportion to simulate the accumulation of fission products), it is applied here due to lack of a specific mixed thorium–uranium oxide model under the assumption that the relative behavior of the materials will be somewhat similar (although this remains to be demonstrated). A similar assumption was made by Long et al. [22] in their development of a $(Th,U)O_2$ model within FRAPCON

$$k_{\text{Lucuta}} = k_0 \boldsymbol{\kappa}_{\mathbf{1d}}(\beta,T)\boldsymbol{\kappa}_{\mathbf{1p}}(\beta,T)\boldsymbol{\kappa}_2(\mathbf{p})\boldsymbol{\kappa}_3(\mathbf{x})\boldsymbol{\kappa}_4(T) \tag{5}$$

$\boldsymbol{\kappa}_{\mathbf{1d}}(\beta,T)$ (Eq. (6)) and $\boldsymbol{\kappa}_{\mathbf{1p}}(\beta,T)$ (Eq. (7)) are the fuel's thermal conductivity dependence on irradiation-induced dislocations and solid fission product precipitates, respectively [26]

$$\boldsymbol{\kappa}_{\mathbf{1d}}(\beta,T) = \left(\frac{1.09}{\beta^{3.265}} + 0.0643\sqrt{\frac{T}{\beta}}\right)\arctan\left(\frac{1}{\frac{1.09}{\beta^{3.265}} + 0.0643\sqrt{\frac{T}{\beta}}}\right) \tag{6}$$

$$\boldsymbol{\kappa}_{\mathbf{1p}}(\beta,T) = 1 + \frac{0.19\beta}{(3 - 0.019\beta)\left(1 + \exp\left(\frac{1200-T}{100}\right)\right)} \tag{7}$$

In Eqs. (6) and (7), β is the burnup in atom percent. A detailed discussion on burnup will follow the description of heat production.

The $\boldsymbol{\kappa}_2(\mathbf{p})$ factor accounts for the dependence on the porosity of the fuel and is outlined in the following equation:

$$\boldsymbol{\kappa}_2(\mathbf{p}) = \frac{1 - \mathbf{p}}{1 + (\mathbf{s} - 1)\mathbf{p}} \tag{8}$$

$\mathbf{s}$ is a porosity shape factor and is set to 1.5 (assuming spherical pores), and $\mathbf{p}$ is the porosity. The porosity is given in the following equation and is the fraction of the fuel's volume that is vacant:

$$\mathbf{p} = 1 - \frac{\rho}{\rho_{\max}} \tag{9}$$

$\rho_{\max}$ is the $(Th,U)O_2$ maximum theoretical density (kg/m^3).

$\boldsymbol{\kappa}_3(\mathbf{x})$ gives the dependence on the deviation from stoichiometry, where $\mathbf{x}$ is the deviation from stoichiometry ($(Th,U)O_{2+x}$). MPM-FAST sets $\boldsymbol{\kappa}_3(\mathbf{x})$ to one, i.e., the model does not consider fuel that is nonstoichiometric. $\boldsymbol{\kappa}_4(T)$ accounts for radiation damage in the fuel, which is annealed at high fuel temperature, as shown in the following equation:

$$\boldsymbol{\kappa}_4(T) = 1 - \frac{0.2}{1 + \exp\left(\frac{T-900}{80}\right)} \tag{10}$$

Finally, Q in Eq. (1) accounts for the heat produced by the fuel (J/(m^3 s)) and is given in the following equation:

$$Q = f_{\text{mag}}\phi \tag{11}$$

f_{mag} is the proportionality coefficient, which ensures that the integrated volumetric heat generation is consistent with the specified linear power:

$$f_{\text{mag}} = \frac{LP}{2\pi\int_0^{P_r}\phi r dr} \tag{12}$$

LP is the linear power (W/m), which is a required input parameter, and P_r is the pellet radius (m).

ϕ is the un-normalized thermal neutron flux profile along the pellet's radius (1/m^2). Within MPM-FAST, the problem of accounting for the changing isotopic composition/flux shape in the fuel pellet is accomplished using the same methods employed by ELESTRES-IST [7,17]. Building new flux depression models for $(Th,U)O_2$ similar to the work of Long et al. [22] is feasible to replicate and is envisioned at a later stage in this work.

The burnup variable (β) is a measure of the fraction of initial heavy element atoms that have undergone fission. Burnup is used to estimate the quantity of fission products within the fuel matrix (see Eq. (5)), and it is also used to briefly describe the fuel after it has undergone irradiation (i.e., at exit burnup). By considering the thermal energy released by fission, burnup can also be measured as the total energy released per initial unit of heavy element. In Canadian PHWR fuel, burnup is typically expressed in 10^6 W h/kgU; for MPM-FAST, the mass of fissile and fertile material is generalized to kilogram of heavy elements (kgHE) to account for fuel composition and will be presented here in J/kgHE. The burnup rate is found using the following equation:

$$\frac{d\beta}{dt} = \frac{Q}{3.6 \times 10^9 \rho_{HE}} \tag{13}$$

ρ_{HE} is the density of the heavy elements (kg/m^3). Other units used to express burnup are atom fraction. The approximate relationship between each of these definitions is 1 atom% $\approx 8.1 \times 10^{11}$ J/kgHE and 1 W h/kgHE $\approx 3.6 \times 10^3$ J/kgHE.

2.2 Deformation. Pellet deformation is accounted for in the second general set of equations applied to both meshed sections of the MPM-FAST geometry. Deformation caused by mechanical loading is described by a pseudo-steady-state equilibrium equation as given in the following equation:

$$-\nabla \cdot \sigma = F_v \tag{14}$$

F_v are the forces acting on the body, in Newtons (N), stored within the material as stress (σ, (Pa)), given by Hooke's Law (with the assumption that the material is isotropic and the stress is linear-elastic) in the following equation:

$$\sigma = [S_{\text{elastic}}][\boldsymbol{\varepsilon}_{\mathbf{elastic}}] \tag{15}$$

$\boldsymbol{\varepsilon}_{\mathbf{elastic}}$ (unitless) is the elastic strain vector and S_{elastic} is the stiffness matrix. Equation (16) is (15) expanded and rearranged to solve for the elastic strain vector in Cartesian coordinates, which are converted to cylindrical while solve for the deformation

$$\begin{bmatrix} \boldsymbol{\varepsilon}_x \\ \boldsymbol{\varepsilon}_y \\ \boldsymbol{\varepsilon}_z \\ \boldsymbol{\gamma}_{xy} \\ \boldsymbol{\gamma}_{xz} \\ \boldsymbol{\gamma}_{yz} \end{bmatrix}_{\mathbf{elastic}} = \begin{bmatrix} 1/E & -\boldsymbol{\nu} & -\boldsymbol{\nu} & 0 & 0 & 0 \\ -\boldsymbol{\nu} & 1/E & -\boldsymbol{\nu} & 0 & 0 & 0 \\ -\boldsymbol{\nu} & -\boldsymbol{\nu} & 1/E & 0 & 0 & 0 \\ 0 & 0 & 0 & 1/G & 0 & 0 \\ 0 & 0 & 0 & 0 & 1/G & 0 \\ 0 & 0 & 0 & 0 & 0 & 1/G \end{bmatrix} \begin{bmatrix} \sigma_x \\ \sigma_y \\ \sigma_z \\ \tau_{xy} \\ \tau_{xz} \\ \tau_{yz} \end{bmatrix} \tag{16}$$

E for Th-based fuels in Pa is given in the following equation:

$$E_{\mathrm{ThO_2}} = E_{\mathrm{ThO_2},273}\mathbf{p}\left(1.023 - 1.405 \times 10^{-4}\, Te^{\frac{-181}{T}}\right) \tag{17}$$

$E_{ThO_2,273}$ is Young's modulus of ThO_2 at 273 K with a value of 249.1 GPa, and **p** is the porosity of the ceramic. Poisson's ratio from Eq. (16), $\boldsymbol{\nu}$, is 0.28 and is unitless.

Both Young's modulus and Poisson's ratio are from Belle and Berman and are based on measurements for ThO_2 [21].

Finally, the shear modulus for an isotropic material (from Eq. (16); G in Pa) can be found using Young's modulus and Poisson's ratio given in the following equation:

$$G = \frac{E}{2(1+\boldsymbol{\nu})} \tag{18}$$

There are additional sources of strain within the materials of a fuel element, such that the elastic strain is found by subtracting the inelastic strain ($\boldsymbol{\varepsilon}_{\mathbf{inelastic}}$) from the total strain ($\boldsymbol{\varepsilon}_{\mathbf{total}}$) given in the following equation:

$$\boldsymbol{\varepsilon}_{\mathbf{elastic}} = \boldsymbol{\varepsilon}_{\mathbf{total}} - \boldsymbol{\varepsilon}_{\mathbf{inelastic}} \tag{19}$$

The axial symmetry implementation in COMSOL assumes that the azimuthal component of the displacement is zero and that there is no change in deformation based on the angular location of the cross section; see Ref. [15] for further details.

The major component of $\boldsymbol{\varepsilon}_{\mathbf{inelastic}}$ is caused by the thermal expansion of the fuel and is known as the thermal strain ($\boldsymbol{\varepsilon}_{\mathbf{thrm}}$). Generally, the temperature behavior of thermal strain is reported directly as a function of temperature; MPM-FAST uses such a temperature-based function for the thermal strain of $(Th,U)O_2$ given in the following equation:

$$\boldsymbol{\varepsilon}_{\mathbf{thrm},(\mathbf{Th},\mathbf{U})\mathbf{O_2}} = \begin{cases} -0.179 - 0.087\mathbf{wtUO_2} + (5.097 + 4.705\mathbf{wtUO_2}) \times 10^{-4}\, T \\ +(3.732 - 4.002\mathbf{wtUO_2}) \times 10^{-7}\, T^2 + (-7.594 + 11.98\mathbf{wtUO_2}) \times 10^{-11}\, T^3 \\ \\ -0.179 - 0.149\mathbf{wtUO_2} + (5.097 + 6.693\mathbf{wtUO_2}) \times 10^{-4} T \\ +(3.732 - 4.002\mathbf{wtUO_2}) \times 10^{-7}\, T^2 + (-7.594 + 19.784\mathbf{wtUO_2}) \times 10^{-11}\, T^3 \end{cases} \tag{20}$$

This correlation for thermal strain was presented in Bakker et al., with the first component valid over the temperature range of 273 K $\leq T <$ 923 K, the second component over the range of 923 K $\leq T <$ 2000 K, and $\mathbf{wtUO_2}$ is the weight fraction of UO_2 in the fuel over the range $0 \leq \mathbf{wtUO_2} \leq 0.1$ [23].

As mentioned earlier, the focus of this work was to outline the models for the physical behavior of $(Th,U)O_2$ that are available in the open literature incorporated into MPM-FAST. There are other sources of inelastic deformation accounted for in FAST that are maintained in MPM-FAST but use the UO_2 models that are available. Table 1 lists these phenomena along with their referenced source; again, the implementation of these models is discussed in Prudil's work [17].

It should be noted that the fracture strength for ThO_2 is presented in Matzke at room temperature [29]. In Matzke's work, the ThO_2 measurements of fracture surface energy and measurements of UO_2 are presented; however, UO_2 measurements were taken at temperatures above room temperature. The ThO_2 fracture surface energy is anywhere from a factor of 2.5 to 12.5 greater than UO_2; however, with the temperature differences between the measurements and unknown effects of porosity, Matzke deemed it inappropriate to make a direct comparison. The fracture model for UO_2 was maintained due to the limited understanding of the fracture strength at operational temperatures. In general, the sensitivity of the solution to the fracture stress is small as a result of the high elastic moduli, leading to relatively small elastic strains compared to inelastic strains.

2.3 Fission Gas. FGR is modeled as a two-stage process: (1) FG concentration is calculated within the grain and the rate at which FG crosses the grain boundary, (2) FG concentration on the grain boundaries and the release of the FG to the gas volume of the element when the concentration exceeds the grain boundary saturation conditions. MPM-FAST tracks the concentration within the fuel grains along the pellet midplane, using a numerical solution to a fully time-dependent Booth diffusion model outlined in Eq. (21), which treats a fuel grain as an idealized homogeneous sphere [30]

$$\frac{\partial FGC}{\partial t} = D\nabla^2 FGC + PR_{fg} \tag{21}$$

FGC is the concentration of FG in the grain in atoms $1/m^3$, PR_{fg} is the volumetric production rate of fission gas in atoms $1/(m^3\ s)$ and is found by multiplying the fission rate by the cumulative yield of

Table 1 List of models that affect deformation that are UO_2 based

Physical phenomena	Sources and notes
Pellet densification	Adapted in Prudil's work from an empirical correlation for Canadian PHWR fuel presented by Floyd et al. [16] and Hastings and Evans [27]
Solid fission product swelling	Burnup-dependent function discussed in Olander [28]
Swelling from grain boundary fission gas bubbles	MATPRO correlation from Luscher and Geelhood altered by Prudil to account for differences in FGR models [10,17]
Pellet fracturing	A pellet cracking model is implemented in FAST and uses the fracture strength of UO_2 given in MATPRO [10]

stable Xe and Kr. MPM-FAST assumes 10% greater FG production during the irradiation of Th-based fuel (compared to UO_2 fuel) due to the fissioning of U-233 producing greater quantities of Kr ([23,24]). Finally, D is the diffusion coefficient of the stable fission gas in the fuel (m^2/s).

In the development of the UO_2 model in FAST, the formulation of D followed Morgan [19]; it was based on the work of Turnbull et al. [31,32], Friskney et al. [33], as well as White and Tucker [34]. For $(Th,U)O_2$, the change in the FG diffusion behavior is scaled by a factor of 0.1 applied to D, as seen in the following equation:

$$D_{(Th,U)O_2} = 0.1D \tag{22}$$

It was found in CNL irradiation experiments that the observed FGR from Th-based fuels is significantly less than that observed in UO_2 fuel [18,35]. During the irradiation test of a defected $(Th,U)O_2$ fuel element, online monitoring of the ^{133}Xe released was found to be 1–2 orders of magnitude less than that of UO_2 fuel. The ingress of coolant into a defected element leads to fuel oxidation in UO_2, which affects the thermal conductivity and microstructure and leads to an increase in FGR. ThO_2 is resistant to steam oxidation, contributing to the retention of fission gas; however, it is uncertain what effect this has for defected Th-based fuel. Some reactions may alter the release rate of ^{133}Xe; however, in post-irradiation annealing tests on thoria–urania fuel (35% ThO_2, 65% UO_2) by Kim et al. [36], it was found that the diffusion of ^{133}Xe in polycrystalline $(Th,U)O_2$ was approximately an order of magnitude less than that of UO_2. These findings provided the rationale for selecting the 0.1 scaling factor for the $(Th,U)O_2$ fission gas diffusion model used. Aside from these measurements, the previous models by Long et al. for $(Th,U)O_2$ light water reactor fuel also applied the assumption of a scaling factor of 0.1 to the high temperature portion of the fission gas diffusion coefficient [24]. A second model developed by Lee et al. for $(Th,U)O_2$ fuel also considered the work of Kim et al. when examining their fission gas release model [37] . This establishes a precedent in terms of approximating the fission gas diffusion of $(Th,U)O_2$ to be one-tenth that of UO_2. These models have also demonstrated an ability to provide fission gas release calculations comparable to measurements of irradiations from a wide range of $(Th,U)O_2$ compositions.

The implementation of the numerical solution of the Booth diffusion equation which provides the release rate of FG to the grain boundary is unaltered from FAST [17]. The second stage of the FGR calculation consists of tracking the concentration of FG on grain boundaries and releasing gas that exceeds grain boundary saturation conditions to the internal volume of the fuel element. The saturated concentration is based on the geometry of the grain boundary bubbles and the maximum observed grain boundary coverage by bubbles [34]. Although the model was developed for UO_2 fuel, extrapolation to $(Th,U)O_2$ is reasonable as it is based on the geometry of grain boundary bubbles (which depends on the effective contact angle from the interfacial energies) and the saturation coverage of the grains (a geometric parameter). Thus, the assumption here is that the contact angle between a FG bubble and the grain boundary is the same as for UO_2 (which can be updated if high-resolution SEM images of irradiated fuel become available).

In MPM-FAST, the average fuel grain diameter is calculated along the midpellet (MP) plane; this is the grain diameter used within the FGR calculation. The $(Th,U)O_2$ model uses of grain growth model proposed by initially by McCauley [38] for porous $(Th,U)O_2$ fuel, based on the work of Nichols [39] on UO_2. This work was then adapted for higher density $(Th,U)O_2$ fuel by Goldberg et al. [40]. The following equation presents this equiaxed grain growth model:

$$PD^3 - PD_i^3 = Kt\,e^{\left(\frac{-V}{RT}\right)} \tag{23}$$

where PD and PD_i are, respectively, the grain diameter and the initial grain diameter within the ceramic fuel pellets (m), t is time (s), R is the universal gas constant (8.314 J/(mol K)), K is a fitting coefficient with a value of 2.88 m^3/s maintained from Nichols' work on UO_2, and V is the vapor activation constant for $(Th,U)O_2$, with a value of 594×10^3J/mol. The value of V was determined for 20–30% wt % UO_2.

3 Modeling Results

Since fuel performance results are sensitive to fuel thermal conductivity, two variations of the $(Th,U)O_2$ MPM-FAST model were examined: case 1 uses Belle and Berman's thermal conductivity correlation [23] and case 2 uses the thermal conductivity presented by Bakker et al. [25]. The model predictions from cases 1 and 2 will be compared to PIE measurements of FGR and end-of-life sheath strain data from DME-221.

DME-221 is an experimental fuel irradiation test conducted by CNL [18]. DME is short hand for "demountable element"; this refers to how the experimental fuel is inserted into the U1 and U2 test loops of the National Research Universal reactor. The experimental fuel was fabricated as elements that are inserted or removed (demounted) from fuel bundle assembly. In the case of DME-221, the bundle has the same geometry as a 37-element Canadian PHWR fuel bundle, the 18 elements in the outer ring house demountable elements, and the center element is removed to allow the bundle to be irradiated in the test loops. Six variations of experimental fuel were fabricated for DME-221: three different fuel compositions (ThO_2, $(Th,U)O_2$ with 1.0 wt % ^{235}U, and $(Th,U)O_2$ with 1.5 wt % ^{235}U) having two different pellet geometries, one set of pellets has a length-to-diameter (L/D) pellet ratio of ~1.3 and the other set has a reduced L/D ratio of ~0.7. Initial average grain size of the fuel was reported as $6–8 \times 10^{-6}$ m, as well as initial densities of ≥95% theoretical density [18]. The DME-221 test is ongoing, 12 elements have undergone PIE, and the three remaining elements will undergo further irradiation. The elements that have undergone PIE were removed on two separate occasions, leading to elements being either a "low" or a "high" exit burnup case. Figures 2–4 are reproduced with permission and display two power histories for each fuel composition that are representative of the low and high exit burnup cases for DME-221 [18].

The maximum modeled centerline temperature, FGR, and end-of-life sheath strain are presented below.

3.1 Centerline Temperature. Table 2 displays a comparison of the highest calculated centerline temperatures between cases 1 and 2 for each DME-221 element.

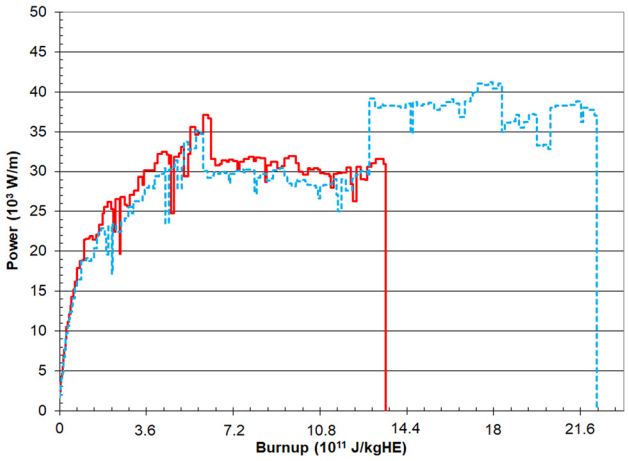

Fig. 2 Power histories for DME-221 ThO_2 fueled elements, with low exit burnup ~1.30×10^{12} J/kgHE and high exit burnup ~2.23×10^{12} J/kgHE [18]

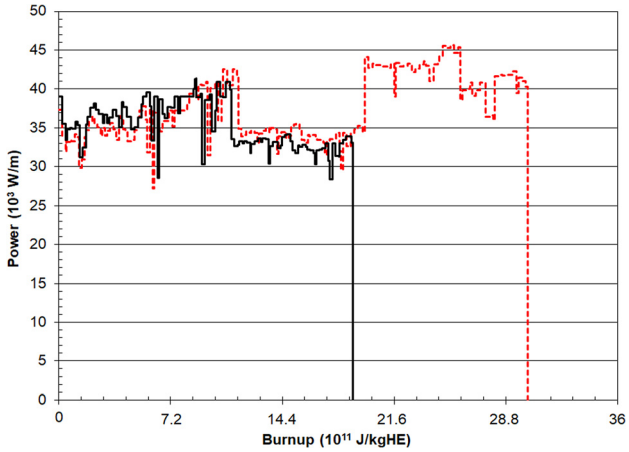

Fig. 3 Power histories for DME-221 (Th,U)O_2 1.0 wt % U-235 fueled elements, with low exit burnup ~ 1.8×10^{12} J/kgHE and high exit burnup ~ 3.0×10^{12} J/kgHE [18]

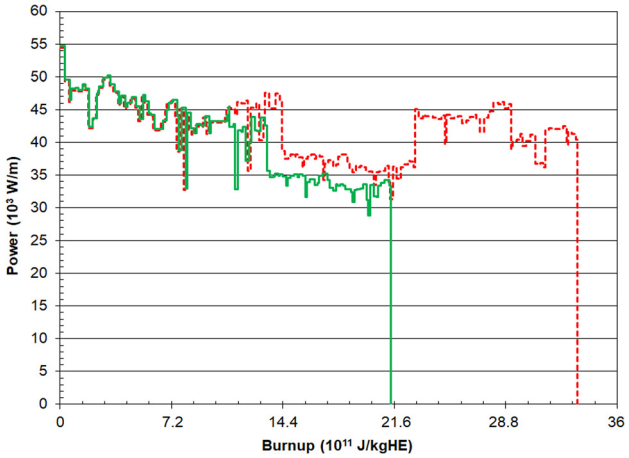

Fig. 4 Power histories for DME-221 (Th,U)O_2 1.5 wt % U-235 fueled elements, with low exit burnup <2.2×10^{12} J/kgHE and high exit burnup >3.2×10^{12} J/kgHE [18]

Centerline temperature results from case 1 are lower than those modeled in case 2. With higher uranium content, the difference in temperature is greater. This temperature difference arises because the Bakker et al. model predicts lower thermal conductivity values for case 2 models compared to the Belle and Berman model (used in case 1). Figure 5 displays the conductivity curves from both models for the 1.5% U-235 fuel (assuming fully dense fuel, porosity is accounted for via Lucuta factor). Consensus within the literature is in favor of using the Bakker correlation [25] over the Belle and Berman correlation [23] due to later measurements displaying larger degradation in thermal conductivity with uranium content than predicted by Belle and Berman [41,42].

In Fig. 5, the vertical lines indicate the uppermost validation temperature for each of the models. It should be noted that many of the high burnup elements in case 2 exceed the maximum temperature for which the Bakker et al. conductivity correlation was developed. This leads to additional uncertainty in the temperature behavior for these cases because it is not known if extrapolating the Bakker correlation is representative in this regime.

As mentioned previously, within the open literature, the expectation is that the Belle and Berman model will predict higher thermal conductivity and may lead to an underprediction of the fuel temperature. Based on this, it is suspected that the modeling results for case 1 fuel temperatures are low. At this time, this suspected behavior cannot be confirmed because DME-221 is not an instrumented fuel test; thus, there are no fuel temperature measurements to validate the modeling results against.

Corbett et al. [18] report that only very limited grain growth occurred in the central region of the 1.5 wt % U-235 elements. Cases 1 and 2 use the grain growth model outlined in Eq. (23). For both sets of results and for all compositions of fuel, the results show no grain growth.

Table 3 compares the difference in fuel performance between the Th-based fuel and UO_2; the results of the Th-based models are given in the middle two columns, and the right most column displays the maximum temperature calculated using the UO_2 model, using the same element geometry and power histories from DME-221.

The Th-based fuel model using either the Belle and Berman correlation or the Bakker et al. thermal conductivity correlation consistently predicts lower centerline temperatures than the UO_2 model. This temperature difference is most pronounced in the high burnup cases. Further demonstrating that there is an improvement in replicating the experimental results using the model presented earlier, the UO_2 model predicts a growth factor 2 for the centerline grains of the 1.5 wt % U-235 fuel. An additional source of error in fuel temperature may be arising from using a flux-depression model that has been developed for UO_2.

3.2 Fission Gas Release. Figure 6 compares the modeled FGR for cases 1 and 2 to measured data [18].

In the validation of FAST, it was found that the model tended to overpredict FGR for UO_2 elements with relatively low measured FGR [21]. With this in mind, case 1 reasonably replicates the ThO_2 with the model overpredicting the upper bound of

Table 2 Comparison of modeled centerline temperatures for DME-221 elements

		Modeled max. temp. DME-221 fuel (K)		
% U-235	Burnup (10^{12} J/kgHE)	Case 1	Case 2	Magnitude of temperature difference (K)
0	1.30	1144	1244	100
0	2.23	1317	1460	143
0	1.35[a]	1174	1281	107
0	2.22[a]	1344	1520	176
1	1.80	1261	1421	160
1	1.89[a]	1315	1411	96
1	3.02[a]	1611	1820	209
1.5	3.34	1698	1860	162
1.5	1.98	1592	1860	268
1.5	2.13[a]	1592	1731	139
1.5	3.29[a]	1669	1831	162
1.5	3.25[a]	1653	1804	151

[a]Fueled with "short" pellets ($L/D = 0.7$).

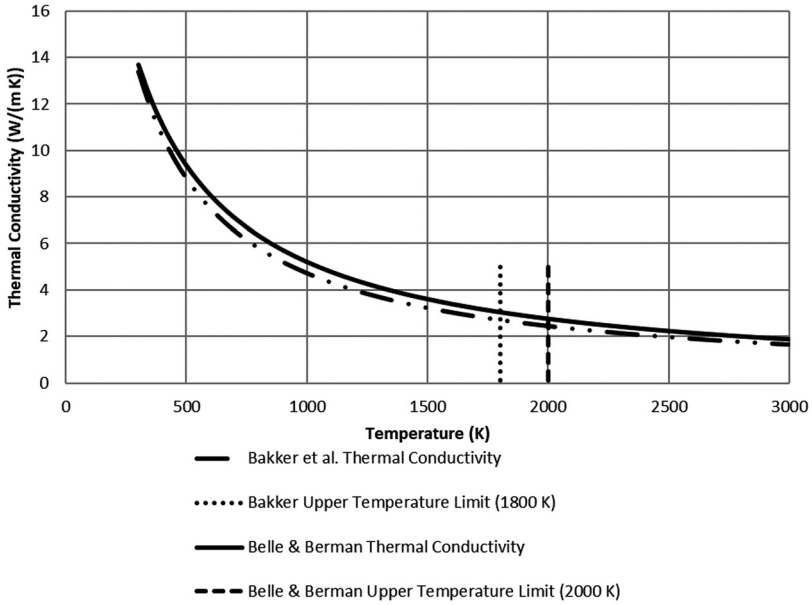

Fig. 5 Comparison of thermal conductivity correlations used in each case for 1.5% U-235 DME-221 fuel

measurement range (0.1% compared to 0.4%), as seen in Fig. 6. By contrast for case 2, the two simulations with predicted gas release exceeded the measured gas releases by at least a factor of 10 for the same irradiation history. Comparing all the low burnup ($<2.2 \times 10^{12}$ J/kgHE) results for both cases 1 and 2, it is similarly observed that case 2 predictions are generally 2–10 times larger than case 1 predictions. For burnups $> 3.2 \times 10^{12}$ J/kgHE, with 1.5% U-235 enriched fuel elements, case 1 models the FGR within the measured range with the exception of the 3.34×10^{12} J/kgHE exit burnup element, which exceeded the measurement range by a relatively small value (modeled 3.3% in comparison to the 2.8% measurement). For case 2, the model exceeded the upper measurement range of the measured data in all three elements. For the 3.34×10^{12} J/kgHE exit burnup element, case 2 predicts 5.0% FGR, almost double the measured FGR. Although the case 2 results for the low burnup fuel elements containing 1.5% U-235 were within the measured data range, none of them reflect the lower bound of the measurement range.

With both models using the fission gas diffusion behavior assumption outlined in Eq. (23), the case 1 model better replicates the FGR behavior of DME-221 fuels. As discussed earlier, it is suspected that the case 1 model will predict lower fuel temperature than case 2 because of its use of the Belle and Berman thermal conductivity correlation. If it is found that the temperature behavior of case 2 models is more physically representative of the fuel temperature, it would suggest that further study of FG diffusion behavior is required to simultaneously produce more realistic fuel temperature and FGR predictions. These changes could include further reductions to the fission gas diffusion coefficient (directly or by modifying the activation energy or athermal terms), or higher grain boundary bubble contact angle or saturation coverage to increase grain boundary retention. At this point in the development and benchmarking of MPM-FAST, it is recommended that the case 1 model be used, as it is better at reproducing the FGR behavior of the DME-221 experiment.

The FGR prediction for the Th-based fuel is improved using MPM-FAST over conventional UO_2 fuel models. As illustrated in Table 4, the FGR calculated by the FAST UO_2 model for UO_2 fueled elements experiencing the same irradiation conditions as the DME-221 fuel is overpredicting the measured values [18].

The FAST UO_2 proof-of-concept validation exercise demonstrated that it produced modeling results in better agreement with PIE data for UO_2 fuel irradiated up to $\sim 2.0 \times 10^{12}$ J/kgU in comparison to ELESTRES [17,21]. However, the Booth equivalent sphere approach which is used in FAST to model FGR does not account for high burnup structures (i.e., rim structure formation) which may become significant at very high powers and high burnups, respectively. The postirradiation analysis did not observe significant restructuring, indicating that the Booth approach may be satisfactory. Further validation and development of NOC models for all fuel compositions would still be beneficial. Regardless both Tables 3 and 4 highlight the advantages of Th-based fuels over conventional UO_2 fuels. The lower temperatures and lower FGR lead to better fuel performance for the same power history.

3.3 Deformation. Modeling results for the sheath strain at the MP region and at the pellet-to-pellet interface (PI) are presented in Tables 5 and 6, respectively, along with the PIE measurements from DME-221 [18].

For the thoria pellets, when the maximum fuel temperature is below 1300 K, both the MP and the PI sheath strain fall within the measurement range. With a burnup of up to 2.2×10^{12} J/kgHE modeled under case 1 conditions, where the fuel temperature does not exceed 1350 K, the deformation calculations agree with the

Table 3 Comparison of the maximum centerline temperature calculated by the $(Th,U)O_2$ models and the UO_2 model

		Modeled max. temp. of fuel (K)		
% U-235	Burnup (10^{12} J/kgHE)	Case 1	Case 2	UO_2
0	1.30	1144	1244	1314
0	2.23	1317	1460	1680
0	1.35[a]	1174	1281	1537
0	2.22[a]	1344	1520	1792
1	1.80	1261	1421	1455
1	1.89[a]	1315	1411	1554
1	3.02[a]	1611	1820	3127
1.5	3.34	1698	1860	2487
1.5	1.98	1592	1860	2921
1.5	2.13[a]	1592	1731	1950
1.5	3.29[a]	1669	1831	2396
1.5	3.25[a]	1653	1804	2386

[a]Fueled with "short" pellets ($L/D = 0.7$).

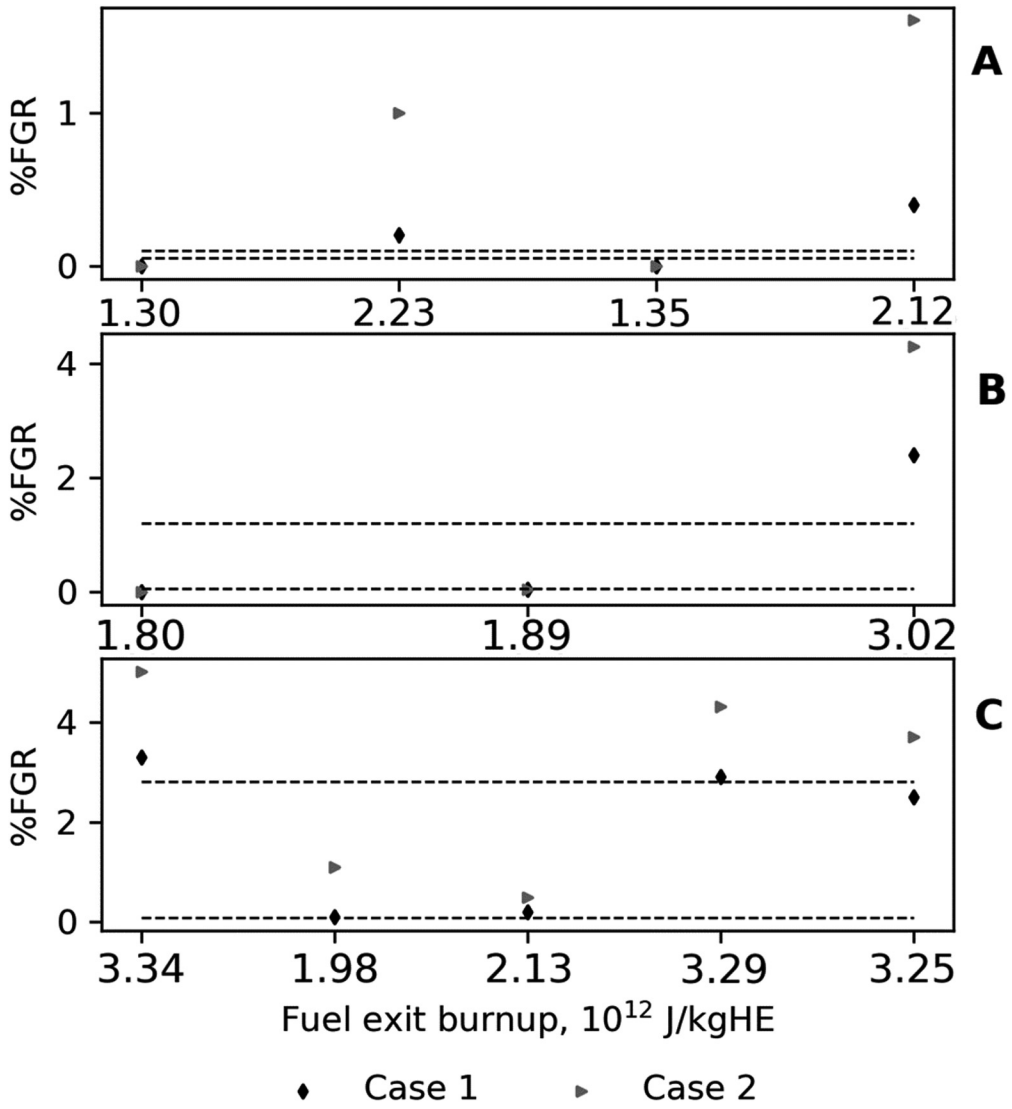

Fig. 6: Comparison of %FGR modeling results to the measurement range from PIE data from DME-221. A—ThO_2 elements, B—1.0% U-235 enriched elements, and C—1.5% U-235 enriched elements with the dashed lines representing the measurement range.

experimental measured range. For fuel containing 1.0 wt % U-235, the models that exceed 1400 K begin to exceed the upper bound of DME-221 results. For fuel centerline temperatures above 1450 K, sheath strains are outside the measured range. Similarly, a fuel temperature of 1650 K appears to be the limit for the 1.5 wt % U-235 fuel. The model begins to overpredict the end-of-life element strains beyond a systematic high temperature limit for each of the fuel compositions. It is difficult to identify the exact cause. A significant number of the models for plastic deformation within the Th-based fuel pellet were adopted from the UO_2 model. An example of this is the gaseous swelling strain since the model is highly dependent on temperature (leading to the observed temperature dependence) and that the fission gas behavior of this fuel is reduced compared to UO_2. This could lead to an overprediction of sheath strain. The Th-based fuel pellet model does not account for creep and axial cracking, the same approach as FAST's UO_2 fuel pellet model. These may also contribute to the discrepancy in deformation results. These results are encouraging as this is a prototype model that has only been benchmarked against limited PIE results.

3.4 Model Uncertainty. Sensitivity analysis for MPM-FAST [15] determined model results was most sensitive to uncertainty in the thermal conductivity correlations. The cases 1 and 2 temperature results agree within their model uncertainties, case 1 FGR results are essentially equal taking measurement error/uncertainty into account but will not account for the deviation in model results to the high burnup cases of end-of-life strain measurements.

Table 4 Comparison of DME-221 PIE FGR results to FAST UO_2 model results

% U-235	Burnup (10^{12} J/kgHE)	Modeled % FGR	Measured % FGR range
0	1.30	0.5	0.05–0.1
0	2.23	15.1	
0	1.35[a]	5.0	
0	2.22[a]	18.1	
1	1.80	5.0	0.06–1.2
1	1.89[a]	6.3	
1	3.02[a]	36.6	
1.5	3.34	22.3	0.08–2.8
1.5	1.98	21.4	
1.5	2.13[a]	10.3	
1.5	3.29[a]	21.1	
1.5	3.25[a]	20.1	

[a]Fueled with "short" pellets (L/D = 0.7).

Table 5 Modeled MP sheath strain compared to PIE data

% U-235	Burnup (10^{12} J/kgHE)	Modeled MP strain (%) Case 1	Case 2	Measured range MP strain (%)
0	1.30	−0.2	−0.1	−0.3 to 0.0
0	2.23	0.08	0.2	
0	1.35[a]	−0.2	−0.1	
0	2.22[a]	0.07	0.2	
1	1.80	−0.03	−0.2	−0.4 to 0.0
1	1.89[a]	−0.04	0.02	
1	3.02[a]	0.4	0.6	
1.5	3.34	0.8	1.0	−0.2 to 0.1
1.5	1.98	0.1	0.4	
1.5	2.13[a]	0.1	0.2	
1.5	3.29[a]	0.6	0.8	
1.5	3.25[a]	0.6	0.7	

[a]Fueled with "short" pellets ($L/D = 0.7$).

Table 6 Modeled PI sheath strain compared to PIE data

% U-235	Burnup (10^{12} J/kgHE)	Modeled PI strain (%) Case 1	Case 2	Measured range PI strain (%)
0	1.30	−0.1	0.02	−0.1 to 0.2
0	2.23	0.2	0.4	
0	1.35[a]	−0.1	0.04	
0	2.22[a]	0.2	0.4	
1	1.80	0.1	−0.2	−0.1 to 0.3
1	1.89[a]	0.1	0.2	
1	3.02[a]	0.7	0.9	
1.5	3.34	1.1	1.4	0.0 to 0.4
1.5	1.98	0.3	0.6	
1.5	2.13[a]	0.3	0.5	
1.5	3.29[a]	0.9	1.2	
1.5	3.25[a]	0.8	1.1	

[a]Fueled with "short" pellets ($L/D = 0.7$).

4 Discussion

4.1 Model Results. Previous (Th,U)O_2 models by Long et al. [24] and Lee et al. [37] elected to use the thermal conductivity model presented by Belle and Berman and were able to produce comparable modeling results to the FGR measurements of irradiated (Th,U)O_2 fuel for light water reactors. Similarly, from the case 1 results presented earlier, MPM-FAST reaffirms that FGR behavior can be replicated using similar assumptions for fission gas diffusion and thermal conductivity. Case 2 models that use the thermal conductivity proposed by Bakker et al. [25] were included to indicate that, despite the availability of physically representative models of FGR, the understanding of high temperature behavior of the thermal conductivity of (Th,U)O_2 continues to evolve and should be included when examining irradiation behavior. From Table 3 for case 2, the model's ability to replicate FGR is limited to the temperature range of the Bakker thermal conductivity correlation. Further examination of the high temperature fission gas diffusion behavior modeling assumptions could be undertaken in attempt to fit case 2 results to the FGR of DME-221. With the fuel centerline temperature exceeding the Bakker et al. thermal conductivity model [25], there is limited confidence that any assumptions made at this time would be correct. It is currently recommended that the Belle and Berman thermal conductivity model be used for fuel temperature calculations because it has been correlated over a larger temperature range.

It should be noted that the models by Long et al. [24] and Lee et al. [37] do not discuss fuel deformation. The applicability of the deformation model in MPM-FAST appears to be limited to lower temperature fuel: ∼1350 K for ThO_2, ∼1450 K for the 1 wt % U-235, and ∼1650 K for the 1.5 wt % U-235 fuel. However, it is a step forward in the development of (Th,U)O_2 fuel performance models with similar capabilities to those expected in a UO_2 model. The current overprediction of fuel swelling (and consequently sheath strain) may serve as bounding estimates for fuel design (at least in the moderate temperature regime).

4.2 Knowledge Gap Assessment. Before the commercialization of Th-based ceramic fuel, fuel performance tools will be required to provide safety analysis. Ideally, these models will be as rigorous as the current tools. Work by Long et al. [43] provided an assessment of the state of knowledge available to model Th-based fuel behavior in NOC and transient conditions for light water reactors in 2004. In the ensuing time, the discussion of the material properties of Th-based ceramic fuel has been re-examined [16,41,42]. New data presented reinforced the correlations that existed in 2004. Table 7 summarizes the thermal physical and mechanical properties used to develop the ThO_2 and (Th,U)O_2 fuel performance model.

Table 7 clearly indicates that the correlations that exist for the unirradiated thermal physical behavior for this fuel type are limited to below 2000 K. While there are methods to infer the behavior of a mixed ceramic fuels from the constituent parts for some properties [41,44], inadequate knowledge persists to support a model of fuel behavior above 2000 K. Reactor designs utilizing higher coolant temperatures (such as the SCWR), reactor transient conditions, or loss of coolant accident scenarios may cause the fuel to exceed 2000 K. This limits the applicability of any fuel model for solid of ThO_2 or (Th,U)O_2 fuel to NOC for current commercial reactor designs.

Even within the context evaluating fuel performance under NOC, there are modeling assumptions that would benefit from further study. Examples such as the irradiation effects on thermal conductivity, pellet deformation, and FG diffusion are discussed below.

Recent development of fuel performance models for (Th,Pu)O_2 fuel have compared model results to online irradiation measurements of the fuel centerline temperature [44,45]. Their results indicate that making similar modeling assumptions about thermal conductivity degradation due to irradiation (U-based degradation model applied to (Th,Pu)O_2) is physically representative, in that the prediction of centerline temperature agrees with the online measurement. Whereas the experiments that the (Th,U)O_2 models have been compared to have been uninstrumented [18,24,37].

Table 7 Thermal physical properties of ThO_2 and (Th,U)O_2 used in model development. Unlisted material properties continue to use the UO_2 models unless specified.

Material property	Source	Temperature correlation limit (K)	Eq. number
Case 1 thermal conductivity	Belle and Berman [23]	2000	(3)
Case 2 thermal conductivity	Bakker et al. [25]	1800	(4)
Young's modulus	Belle and Berman [23]	1600	(17)
Thermal expansion	Bakker et al. [25]	2000	(20)
Heat capacity	Cognet et al. [41]	2000	N/D[a]

[a]N/D- Not discussed.

Similar experimental verification is not available for the $(Th,U)O_2$ fuel. The evidence from the $(Th,Pu)O_2$ experience provides some reassurance that it appears to be a reasonable assumption. Given that many of the processes within the fuel are temperature driven, any means of ensuring a physically representative temperature calculation would strengthen the model. Experimental reassurance could be obtained either from an instrumented fuel irradiation or by measuring the thermal resistivity of the irradiated fuel from the experiments used for the model comparisons.

The MPM-FAST results for end-of-life sheath strain demonstrate that modeling $(Th,U)O_2$ deformation, while reflective of the general behavior, is not entirely physically representative. Table 1 lists the inelastic deformation models that are carried over from the UO_2 model. Four of the phenomena are associated deformation that is irradiation driven, while the fifth is pellet fracturing. Within these phenomena, models lie as the likely cause of the modeling discrepancy. Further sensitivity analysis could be focused specifically on these models to determine the most likely phenomena responsible. However, experimental evidence would still be required to validate any modeling assumption.

The primary evidence that has motivated the modeling assumption for changing the FG diffusion coefficient in this work and other similar models has primarily been related to measurements of integrated FGR from irradiation experiments [18,24,35,37]. The work performed by Turnbull et al. [31,32] and Friskney et al. [33] determined single fission gas atom diffusion coefficients for UO_2 through experimentation. The direct observation of each effect allowed for the temperature over which it is dominant. With Th-based ceramics being more refractory, the activation energy of diffusion and gas trapping processes in Th-based fuel may be substantially different. While the work of Kim et al. [36] begins to address thermally activated diffusion in $(Th,U)O_2$, further experiments examining FG diffusion in Th-based grains would improve the FG diffusion model. The complex temperature dependence can be difficult to obtain from integral fuel performance experiments due to the nonlinear coupling between material properties and irradiation conditions. As such, separate effects studies may be more suitable for analyzing the temperature dependence.

In summary, the MPM-FAST ThO_2 and $(Th,U)O_2$ model is not as robust as the FAST UO_2 model (and many other UO_2-based fuel performance models). This is a reflection of the overall understanding of the irradiation and high temperature behavior of $(Th,U)O_2$ in comparison to the understanding of UO_2 fuel performance. If there is to be a fuel performance model available to perform safety analysis calculations for commercialized $(Th,U)O_2$, substantial effort must be focused on expanding the understanding of the high temperature irradiation behavior of $(Th,U)O_2$ to make it comparable to the abilities of UO_2 models. Efforts in Canada to address these gaps are outlined by Floyd et al. [16].

5 Conclusions

A prototype for a ThO_2 and $(Th,U)O_2$ fuel performance model (MPM-FAST) has been developed as part of the research into the Canadian SCWR concept for GEN-IV forum. Two cases of the model were examined using different correlations for the thermal conductivity of $(Th,U)O_2$, with the model results compared to measured data from the DME-221 fuel irradiation test conducted in CNL's NRU reactor. It was found that one case provided a good approximation for FGR. At this time, the model that uses the Belle and Berman thermal conductivity model is recommended, because it better replicates the FGR observed in the DME-221 irradiation test. Both configurations of the model tended to overpredict end-of-life sheath strain. Deformation predictions were in better agreement with measurements for elements that experienced lower maximum temperatures. This underscores the state of overall understanding of the high temperature and irradiation behavior of ThO_2 and $(Th,U)O_2$ nuclear fuel.

Acknowledgment

Funding to the Canada Gen-IV National Program was provided by Natural Resources Canada through the Office of Energy Research and Development, Atomic Energy of Canada Limited, and Natural Sciences and Engineering Research Council of Canada.

The authors would like to thank CNL staff Holly Hamilton (since retired), Jeremy Pencer, Bill Richmond, Stavros Corbett, Ian Lusk (since retired), Tony Williams, and Mark Floyd for their assistance in preparing this paper and continued collaboration on the model described in it.

Nomenclature

Greek Symbols (Including Non-Dimensional Numbers in Bold)

β = burnup, J/kgHE or atom %
$\boldsymbol{\gamma}$ = strain of off axial components
$\boldsymbol{\varepsilon}$ = strain along directional axes
$\boldsymbol{\kappa}$ = component of Lucuta thermal conductivity model
$\boldsymbol{\nu}$ = Poisson's ratio
ρ = density, kg/m^3
σ = stress, Pa
τ = off axial components of stress, Pa

Superscripts/Subscripts

A = fitting correlations for $(Th,U)O_2$ from Belle and Berman
B = fitting correlations for $(Th,U)O_2$ from Bakker et al.
elastic = elastic component of strain
fg = fission gas
HE = heavy elements
i = initial value
inelastic = inelastic component of strain
Lucuta = indicates Lucuta model to account for irradiation effects on thermal conductivity
Max = maximum value
p = constant pressure
r = radius
ThO_2 = material property of thoria
thrm = thermal component of strain
$(Th, U)O_2$ = material property of thorium uranium dioxide
Total = total acting on body
v = acting on the volume of a body
x = acting along the x-axis
xy = acting along off axial xy component
xz = acting along off axial xz component
y = acting along the y-axis
yz = acting along off axial yz component
z = acting along the z-axis
0 = indicates unirradiated thermal conductivity
1d = Lucuta model component for dependence on irradiation induced dislocations
1p = Lucuta model component for dependence on solid fission product precipitates
2 = Lucuta model component for dependence on the porosity of the fuel
3 = Lucuta model component for dependence on the porosity of the fuel
4 = Lucuta model component for dependence on radiation damage in the fuel
273 = value at 273 Kelvin

Acronyms/Abbreviations

CNL = Canadian Nuclear Laboratories
FAST = fuel and sheath modeling tool

FG = fission gas
FGR = fission gas release
L/D = length to diameter ratio
MP = midpellet
MPM-FAST = multipellet material FAST
N/D = not discussed
NOC = normal operating conditions
PHWR = pressurized heavy water reactors
PI = pellet-to-pellet interface
PIE = postirradiation examination
RMCC = Royal Military College of Canada
SCWR = supercritical water-cooled reactor
wt % = percent by weight

Chemical Formulae and Name

ThO_2 = thoria
$(Th,Pu)O_2$ = thorium plutonium dioxide
$(Th,U)O_2$ = thorium uranium dioxide
UO_2 = uranium dioxide

Nondimensional Numbers

A = semi-empirical fitting factor for k_0
B = semi-empirical fitting factor for k_0
p = porosity of ceramic
s = shape factor of pores in ceramic
wtUO$_2$ = weight fraction of UO_2 in the fuel

Parameters With Dimensions

C = heat capacity, J/(K kg)
D = diffusion coefficient of fission gas, m^2/s
E = Young's modulus, Pa
F = forces acting on the body, N
FGC = concentration of fission gas atoms ($1/m^3$)
G = shear modulus, Pa
k = total thermal conductivity, W/(m K)
K = Th-based grain growth fitting constant, m^3/s
LP = linear power, W/m
P = pellet radius, m
PD = average grain diameter, m
Q = volumetric heat production rate, J/(m^3 s)
R = Universal gas constant, J/(mol K)
t = time, s
T = temperature, K
V = vapor activation constant for $(Th,U)O_2$, J/mol

References

[1] McDonald, M. H., Hyland, B., Hamilton, H., Leung, L. K. H., Onder, N., Pencer, J., and Xu, R., 2011, "Pre-Conceptual Fuel Design Concepts for the Canadian Super Critical Water-Cooled Reactor," Fifth International Symposium on Supercritical Water-Cooled Reactors (ISSCWR-5), Vancouver, BC, Canada, Mar. 13–16, Paper No. P134.
[2] Yetisir, M., Diamond, W., Leung, L. K. H., Martin, D., and Duffer, R., 2011, "Conceptual Mechanical Design for a Pressure-Tube Type Supercritical Water-Cooled Reactor," Fifth International Symposium on Supercritical Water-Cooled Reactors (ISSCWR-5), Vancouver, BC, Canada, Mar. 13–16, Paper No. P055.
[3] Kuran, S., Hopwood, J., and Hastings, I. J., 2011, "Fuel Cycles–A Key to Future CANDU Success," International Conference on Future of Heavy Water Reactors Proceedings, Ottawa, ON, Canada, Oct. 2–5, Paper No. 026.
[4] BARC, 2016, "About Us:ANUSHAKTI—Atomic Energy In India: Strategy for Nuclear Energy - BARC," Bhabha Atomic Research Centre, Department of Atomic Energy, Government of India, Mumbai, India, accessed Oct. 16, 2016, http://barc.gov.in/about/anushakti_sne.html
[5] World Nuclear News, 2016, "Canada and China Team up on AFCR," World Nuclear News, accessed Oct. 16, 2016, http://www.world-nuclear-news.org/C-Canada-and-China-team-up-on-AFCR-2309164.html
[6] Thorbeck, A., 2016, "Startpage," Thor Energy, Oslo, Norway, accessed Oct. 16, 2016, http://thorenergy.no/
[7] Chassie, G. G., Sim, K. S., Wong, B., and Papayiannis, G., 2005, "ELESTRES Code Upgrades," Ninth International Conference on CANDU Fuel, 'Fuelling a Clean Future', Bellville, ON, Canada, Sept. 18–21, Paper No. C3001.
[8] Williams, A. F., 2005, "The ELOCA Fuel Modelling Code: Past, Present and Future," Ninth International Conference on CANDU Fuel, 'Fuelling a Clean Future', Bellville, ON, Canada, Sept. 18–21, Paper No. B4007.
[9] Geelhood, K. J., Luscher, W. G., and Beyer, C. E., 2011, "FRAPCON-3.4: A Computer Code for the Calculation of Steady-State, Thermal-Mechanical Behavior of Oxide Fuel Rods for High Burnup (NUREG/CR-7022, Volume 1, PNNL-19418, Volume 1)," Nuclear Regulatory Commission, Richland, WA, Report No. PNNL-19418.
[10] Luscher, W. G., and Geelhood, K. J., 2011, "Material Property Correlations: Comparisons Between FRAPCON-3.4, FRAPTRAN 1.4, and MATPRO," Nuclear Regulatory Commission, Richland, WA, Report No. PNNL-19417.
[11] Lyon, W., Montgomery, R., Zangari, A., Sunderland, D., Rashid, Y., and Dunham, R., 2002, "Fuel Performance Analysis Capability in Falcon," Nucl. Eng. Des., **295**, pp. 910–921.
[12] Lassmann, K., 1992, "TRANSURANUS: A Fuel Rod Analysis Code Ready for Use," J. Nucl. Mater., **188**, pp. 295–302.
[13] Baurens, B., Sercombe, J., Riglet-Martial, C., Desgranges, L., Trotignon, L., and Maugis, P., 2014, "3D Thermo-Chemical–Mechanical Simulation of Power Ramps With ALCYONE Fuel Code," J. Nucl. Mater., **452**(1–3), pp. 578–594.
[14] Newman, C., Hansen, G., and Gaston, D., 2009, "Three Dimensional Coupled Simulation of Thermomechanics, Heat, and Oxygen Diffusion in Nuclear Fuel Rods," J. Nucl. Mater., **392**(1), pp. 6–15.
[15] Bell, J. S., 2017, "Thorium-Based Nuclear Fuel Performance Modelling With Multi-Pellet Material Fuel and Sheath Modelling Tool," Ph.D. thesis, Royal Military College of Canada, Kingston, ON, Canada.
[16] Floyd, M. R., Bromley, B., and Pencer, J., 2016, "A Canadian Perspective on Progress in Thoria Fuel Science and Technology," CNL Nucl. Rev., **6**(1), pp. 1–17.
[17] Prudil, A., 2013, "FAST: A Fuel and Sheath Modeling Tool for CANDU Reactor Fuel," Ph.D. thesis, Royal Military College of Canada, Kingston, ON, Canada.
[18] Corbett, S., Floyd, M. R., Livingstone, S. J., Hamilton, H., and Harrison, N. F., 2013, "DME-221 Thoria Fuel: Fabrication, Irradiation Testing, and Post-Irradiation Examination," 12th International CANDU Fuel Conference Proceedings, Kingston, ON, Canada, Sept. 15–18, pp. 1–14.
[19] Morgan, D., 2007, "A Thermomechanical Model of CANDU Fuel," M.S. thesis, Royal Military College of Canada, Kingston, ON, Canada.
[20] Shaheen, K., 2011, "A Mechanistic Code for Intact and Defective Nuclear Fuel Element Performance," Ph.D. thesis, Royal Military College of Canada, Kingston, ON, Canada.
[21] Prudil, A., Lewis, B. J., Chan, P. K., and Baschuk, J. J., 2015, "Development and Testing of the FAST Fuel Performance Code: Normal Operating Conditions—Part 1," Nucl. Eng. Des., **282**, pp. 158–168.
[22] Prudil, A., Lewis, B. J., Chan, P. K., Baschuk, J. J., and Wowk, D., 2015, "Development and Testing of the FAST Fuel Performance Code: Transient Conditions—Part 2," Nucl. Eng. Des., **282**, pp. 169–177.
[23] Belle, J., and Berman, R. M., 1984, "Thorium Dioxide: Properties and Nuclear Applications," USDOE Assistant Secretary for Nuclear Energy, Naval Reactors Office United States Department of Energy, Pittsburgh, PA, Report No. DOE/NE–0060.
[24] Long, Y. Y. Y., Kazimi, M. S., Ballinger, R. G., and Pilat, E. E., 2002, "A Fission Gas Release Model for High-Burnup LWR ThO_2-UO_2 Fuel," Nucl. Technol., **138**(3), pp. 260–272.
[25] Bakker, K., Cordfunke, E. H. P., Konings, R. J. M., and Schram, R. P. C., 1997, "Critical Evaluation of the Thermal Properties of ThO_2 and Th1−yUyO_2 and a Survey of the Literature Data on Th1−y$PuyO_2$," J. Nucl. Mater., **250**(1), pp. 1–12.
[26] Lucuta, P. G., Matzke, H., and Hastings, I. J., 1996, "A Pragmatic Approach to Modelling Thermal Conductivity of Irradiated UO_2 Fuel: Review and Recommendations," J. Nucl. Mater., **232**(2–3), pp. 166–180.
[27] Hastings, I. J., and Evans, L. E., 1979, "Densification Algorithm for Irradiated UO_2 Fuel," J. Am. Ceram. Soc., **62** (3–4), pp. 217–218.
[28] Olander, D. R., 1976, "Fundamental Aspects of Nuclear Reactor Fuel Elements," California University, Berkeley, CA, Report No. TID-26711-P1.
[29] Matzke, H., 1980, "Hertzian Indentation of Thorium Dioxide, ThO_2," J. Mater. Sci., **15**(3), pp. 739–746.
[30] Booth, A. H., 1957, "A Method of Calculating Fission Gas Release From UO_2 Fuel and Its Application to the X-2-F Loop Test," Atomic Energy of Canada Limited, Chalk River, ON, Canada, Report No. AECL-496.
[31] Turnbull, J. A., Friskney, C. A., Johnson, F. A., Walter, A. J., and Findlay, J. R., 1977, "The Release of Radioactive Gases From Uranium Dioxide During Irradiation," J. Nucl. Mater., **67**(3), pp. 301–306.
[32] Turnbull, J. A., Friskney, C. A., Findlay, J. R., Johnson, F. A., and Walter, A. J., 1982, "The Diffusion Coefficients of Gaseous and Volatile Species During the Irradiation of Uranium Dioxide," J. Nucl. Mater., **107**(2–3), pp. 168–184.
[33] Friskney, C. A., Turnbull, J. A., Johnson, F. A., Walter, A. J., and Findlay, J. R., 1977, "The Characteristics of Fission Gas Release From Monocrystalline Uranium Dioxide During Irradiation," J. Nucl. Mater., **68**(2), pp. 186–192.
[34] White, R. J., and Tucker, M. O., 1983, "A New Fission-Gas Release Model," J. Nucl. Mater., **118**(1), pp. 1–38.
[35] Livingstone, S. J., and Floyd, M. R., 2013, "Thoria Irradiation and Post-Irradiation Examination Experience at AECL," 12th International CANDU Fuel Conference, Kingston, ON, Canada, Sept. 15–18, pp. 1–11.
[36] Kim, H., Park, K., Kim, B. G., Choo, Y. S., Kim, K. S., Song, K. W., Hong, K. P., Kang, Y. H., and Ho, K., 2004, "Xenon Diffusivity in Thoria-Urania Fuel," Nucl. Technol., **147**(1), pp. 149–156.

[37] Lee, C. B., Yang, Y. S., Kim, Y. M., Kim, D. H., and Jung, Y. H., 2004, "Irradiation Behavior of Thoria-Urania Fuel in a PWR," Nucl. Technol., **147**(1), pp. 140–148.
[38] McCauley, J. E., 1969, "Observations on the Irradiation Behavior of a Zircaloy-4 Clad Rod Containing Low Density ThO_2—5.3 W/O UO_2 Pellets (LWBR Development Program)," Bettis Atomic Lab, Pittsburgh, PA, Technical Report No. WAPD-TM-664.
[39] Nichols, F. A., 1968, "Further Comments on the Theory of Grain Growth in Porous Compacts," J. Am. Ceram. Soc., **51**(8), pp. 468–468.
[40] Goldberg, I., Waldman, L. A., Giovengo, J. F., and Campbell, W. R., 1979, "Fission Gas Release and Grain Growth in ThO_2-UO_2 Fuel Irradiated at High Temperature," Bettis Atomic Lab, Pittsburgh, PA, Technical Report No. WAPDTM-1350.
[41] Cognet, G., Efanov, A., Fortov, V., Fink, J. K., Froment, K., Gromov, G., Hwang, I. S., Jaroma-Weiland, G., Jeong, K. J., Jiang, Y., Kim, Y. S., Mares, R., Matthew, P. M., Petoukhov, V., Piluso, P., Sengupta, A. K., Venugopal, V., and Vinogradov, V., 2006, *Thermophysical Properties Database of Materials for Light Water Reactors and Heavy Water Reactors*, International Atomic Energy Agency, Vienna, Austria.
[42] Konings, R., 2012, *Comprehensive Nuclear Materials*, Elsevier, Amsterdam, The Netherlands.
[43] Long, Y., Siefken, L. J., Hejzlar, P., Loewen, E. P., Hohorst, J. K., MacDonald, P. E., and Kazimi, M. S., 2004, "The Behavior of ThO_2-Based Fuel Rods During Normal Operation and Transient Events in LWRs," Nucl. Technol., **147**(1), pp. 120–139.
[44] Insulander Björk, K., and Kekkonen, L., 2015, "Thermal–Mechanical Performance Modeling of Thorium–Plutonium Oxide Fuel and Comparison With On-Line Irradiation Data," J. Nucl. Mater., **467**(Pt. 2), pp. 876–885.
[45] Boer, B., Lemehov, S., Wéber, M., Parthoens, Y., Gysemans, M., McGinley, J., Somers, J., and Verwerft, M., 2016, "Irradiation Performance of $(Th,Pu)O_2$ Fuel Under Pressurized Water Reactor Conditions," J. Nucl. Mater., **471**, pp. 97–109.